Highly twisted carbazole-borane derivatives: B–N stereodynamic analysis and consequences on their emission properties

ARTICLE

Highly twisted carbazole-borane derivatives. B-N Stereodynamic analysis and consequences on their emission properties.

Received 00th January 20xx,
Accepted 00th January 20xx

DOI: 10.1039/x0xx00000x

Daniel Pecorari,[a] Andrea Mazzanti,[a] Stefano Gianvittorio,[a] Simone Foschi,[a] Stefano Stagni,[a] Valentina Fiorini,[a] and Michele Mancinelli.*[a]

The stereodynamic properties of amino bis-mesityl-boranes bearing carbazole and benzocarbazole as the donor heterocycle have been investigated by dynamic NMR analysis and simulated by DFT calculations. The π-contribution to the B-N bond has been measured as 24 kcal/mol when carbazole is the donor heterocycle, while a value of 21.7 kcal/mol was determined for the benzocarbazole series. On these basis, two rotational barriers were determined for the B-N bond, the lower one (11.1-16.9 kcal/mol) leading to conformational enantiomers, and the higher one (21.0-24.0 kcal/mol) likely being responsible for the E-Z isomerization in compound bearing different aryl rings bound to the boron atom. It has been shown that both kinds of dynamic rearrangement involve a correlated motion of all the three rings. The difference in the ground state geometries and the different π-contribution led to pronounced variations in the fluorescence spectra, due to different geometric rearrangements in the TICT excited state. Stokes shift larger than 10000 cm^{-1} was observed in the carbazole series, with quantum yields up to 50%. It has been found that the π-contribution to the B-N bond in the excited state is still significant, with B-N isomerism likely not taking place in the ns scale.

Introduction

Amino-boranes are a new class of "smart materials",[1] useful for specialized and practical applications, owing to their low cost and their peculiar properties. They have a broad range of applications for their luminescent properties, such as OLEDs,[2] solid-state mechanofluorochromism,[3] fluorescent probes[1] and organoboron-based materials in nonlinear optics.[4] Isosteric and isoelectronic to a classic C=C double bond, the B-N bond allows for amino-boranes to respond to external stimuli such as solvent, temperature, and others.[5] Another interesting property is the high emission quantum yield in the solid state and in solution, where a rise in the concentration or the addition of a non-solvent leads to aggregation induced emission (AIE).[6]

Although methyl substituents in *ortho* positions of the aryls protect the boron from nucleophilic attack, simple tris-aryl boron without any ortho substituent on the aryl rings usually exhibit poor chemical stability due to the empty p_z-orbital on boron atom. On the contrary, chemically stable amino-boranes can be prepared *via* the addition of a Lewis base (i.e. an amine) to bis-aryl boron fluoride. The combination of the filled p_z-orbital on nitrogen with the empty p_z-orbital of boron generates a π-conjugated scaffold that enhances the chemical stability, also determining a small HOMO-LUMO gap. This feature implies that amino-boranes are usually brightly fluorescent, with large Stokes-shifts,[3b] being these effects further amplified by the presence of bulky and structurally rigid aryl groups in close proximity to the boron atom. Recently, the occurrence of thermally assisted delayed fluorescence (TADF) was described for bulky carbazoles with donor methoxy substituent.[7] Irle reported DFT and TD-DFT calculations on twisted internal charge transfer (TICT),[8] to investigate the effects of modifications of the ground state geometries (and of the electronic features on the carbazole) on the TICT rearrangement.

Although the fluorescence properties have been studied in recent years, the dynamic analysis of these systems, as well the consequences of fluorescence properties driven by ground state (GS) geometry modifications, have not been investigated yet. Over the past years, the stereochemistry and dynamic analysis of organic boron compounds such as triarylboranes, have attracted considerable attention from many researchers. In particular, Mislow and co-workers pioneered several researches on the dynamic stereochemistry of tris-arylboranes in the 70s, disclosing many fundamental concepts of dynamic stereochemistry.[9]

Due to the asymmetry of the electron distribution, the π-bond of the B-N moiety has different properties with respect to a standard alkene. Some years ago, Dixon predicted a value of 29.9 kcal/mol for the rotation of the simplest amine-borane.[10] This value is directly related to the strength of the π-bond, that has to be broken to achieve rotation through a transition state

[a] *Department of Industrial Chemistry "Toso Montanari", University of Bologna, Viale del Risorgimento 4, I-40136 Bologna, Italy*

† Footnotes relating to the title and/or authors should appear here.

Electronic Supplementary Information (ESI) available: [details of any supplementary information available should be included here]. See DOI: 10.1039/x0xx00000x

(TS) geometry where the plane of amine and that of borane are mutually perpendicular. In this manuscript we present the preparation of some carbazole- and benzocarbazole- amino boranes (Scheme 1) showing conformational properties that allowed to measure the π-contribution to the B-N bond, both in the ground state and excited state, and how different electronic and steric contributions modify the electronic features and the photophysical properties.

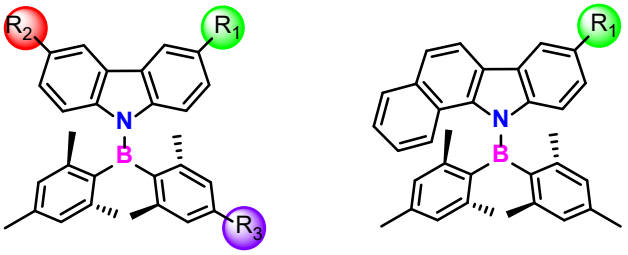

1 R_1=R_2=H R_3 = Me
2a R_1=*i*-Pr R_2=H R_3 = Me
2b R_1=*i*-Pr R_2=H R_3 = H
3 R_1=*i*-Pr R_2=OMe R_3 = Me
4 R_1=*i*-Pr R_2=CF_3 R_3 = Me

5 R_1=H
6 R_1=*i*-Pr
7 R_1=OMe
8 R_1=CF_3

Scheme 1. Prepared compounds.

Compounds **2a** and **3-8** were prepared by addition of the respective carbazole potassium salt to previously prepared Mes_2BF.[11] Compound **2b** was prepared following a different procedure to obtain the intermediate Mes-Xyl-BF (see experimental part in SI). The isopropyl moiety was added to the carbazole scaffold (**1-4**) to have a stereochemical probe that can reveal the formation of conformational chirality by monitoring the methyl signals with NMR spectroscopy. The electronic effects on emission properties were investigated adding to the heterocycle an electron-donating group (EDG, -OMe, **3**,**7**) or an electron-withdrawing group (EWG, $-CF_3$, **4**,**8**).

Results and discussion

Conformational analysis and calculations

In known phenothiazine-bis-mesityl boron compounds,[3a] the antiaromatic phenothiazine ring is rather flexible and it can bend to better allocate the steric hindrance of the *ortho* methyl groups of the mesityl rings. This allows the two p_z-orbitals on nitrogen and boron to reach a quasi-parallel disposition (AIE emission has been proposed as due to the freezing of the ring flip in the aggregates). Indeed, the C_b-N-B-C_e torsion angle (ϕ_1) is 20°. When the phenothiazine ring is substituted by the carbazole ring, the stiffness of the heteroaromatic system changes the whole system.[11]

From the conformational point of view, these bis-aryl-aminoboranes contains two different stereochemical substructures: 1) the two mesityl groups bound to the sp^2-hybridized boron atom; 2) the aromatic amine bound to boron generating the B-N π-system (see Scheme 2 for definition of bond and torsion angles). The first stereodynamic system is strongly related to known compounds such as bis-mesityl ketone and 1,1-bis-mesitylethylene, whose dynamic stereochemical behaviour has been analysed in detail.[12]

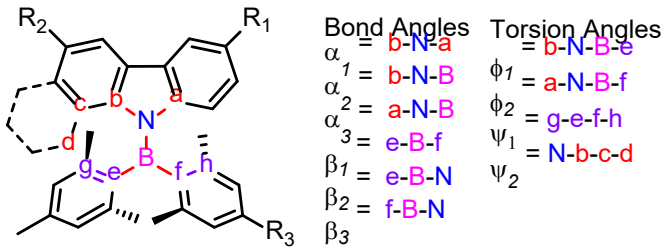

Scheme 2.

Within this system, the rotations of the two mesityl rings are geared together (ψ_1 in Scheme 2), with a single transition state for the rotation of both the two aryl rings. In mesityl ketone, this correlated rotation has a very low activation energy because of the high energy of the GS, and because gearing lowers the TS energy[13]. In the present case, the longer B-C bond and the different electronic features of the sp^2 system likely cause a different outcome, due to the different stabilization of the GSs and TSs.[14] While the longer B-C bond length should reduce the steric hindrance among the *ortho* methyls of the mesityl rings in the GS (thus raising the rotational barrier), the effects in the TS energy are not easy to predict. The second stereochemical system is the rotation around the B-N bond (ϕ_1 and ϕ_2). Analogously with amides, when the two p_z orbitals of boron and nitrogen are parallel (i.e. $\phi_1 \approx \phi_2 \approx 0$), the π conjugation reaches its maximum. The 180° rotation of the heterocycle implies a complete loss of conjugation in a TS geometry where the C_b-N-C_a plane (and the p_z orbital on nitrogen) is perpendicular to the C_e-B-C_f one (and to the empty p_z orbital on boron). In analogy with the terminology used for biphenyl systems,[15] this geometry corresponds to the so-called "conjugative barrier". The experimental measurement of the B-N rotational barrier can provide an accurate measurement of the π contribution on the B-N moiety, compared with that of a standard C=C bond. On the other hand, the carbazole ring is rigid and very close to the steric hindrance exerted by the two mesityl rings. In particular, H1 and H8 of carbazole point toward the two *ortho* methyls of the mesityl rings. This forces a geometry distortion of the heterocycle to better arrange the steric hindrance of the mesityl rings, resulting in an out-of-the-plane displacement (ϕ_1 and $\phi_2 \neq 0$, see Figure 1 and Table 1), with a not perfect alignment of the p_z orbitals on boron and nitrogen. This situation can be again related to biphenyl, where the skewed GS geometry is the result of the attempt to achieve conjugation and the need to accommodate the *ortho* hydrogens far from each other. From this point of view these amino-boranes are related to overcrowded alkenes, where light-excitation achieves highly effective configurational isomerism.[16] The overall ground state geometry of compound **1** belongs to the C_2 symmetry point, implying the formation of a pair of conformational enantiomers. This arrangement also implies a second rotational barrier ("steric barrier" in analogy with biphenyl), due to the exchange between the conformational enantiomers *via* a transition state where ϕ_1 and ϕ_2 torsion angles are very close to 0° (i.e. the B-N

π bond reaches the best conjugation but also the highest steric hindrance).

DFT calculations were run on compound **1** to investigate its conformational preferences. Calculations at the B3LYP/6-311G(d,p) level of theory[17] suggested that the ϕ_1 and ϕ_2 torsion angles in the ground state are both 28° (23.1° experimental value[Errore. Il segnalibro non è definito.]), and both boron and nitrogen are planar ($\alpha_1+\alpha_2+\alpha_3=360$, $\beta_1+\beta_2+\beta_3=360°$). When the heteroaromatic ring is asymmetrically substituted (compounds **2-8**), the ground state geometry belongs to the C_1 symmetry point group. Scheme 2 summarizes the theoretical results for compounds **1-8**.

Table 1 Calculated geometries for compounds **1-8**, calculated at the B3LYP/6-311G(d,p) level of theory**.**

Compd.	B-N (Å)	$\beta_1+\beta_2+\beta_3$	$\alpha_1+\alpha_2+\alpha_3$	ϕ_1	ϕ_2	ψ_1	ψ_2
1	1.45	360.0	360.0	-27.9	-27.9	-156.6	-
2a	1.45	360.0	360.0	-27.6	-27.4	-157.0	-
***E*-2b**	1.45	360.0	360.0	-27.5	-27.2	-157.3	-
***Z*-2b**	1.45	360.0	360.0	-27.2	-27.5	-157.2	-
3	1.45	360.0	360.0	-26.5	-27.1	-157.6	-
4	1.45	360.0	360.0	-28.2	-28.2	-155.5	-
5	1.47	360.0	357.6	-26.5	-44.1	-147.7	-5.5
6	1.46	360.0	357.6	-25.9	-43.5	-148.4	-5.5
7	1.46	359.9	357.7	-26.0	-43.2	-148.4	-5.5
8	1.47	360.0	357.8	-27.9	-44.8	-146.3	-5.2

Within the carbazole series, boron and nitrogen are planar, and the skew angles are close to 27°. On the contrary, the higher steric hindrance caused by benzocarbazole in compounds **5-8** raises one of the skew angles (ϕ_2) and the nitrogen atom is made slightly pyramidal.

The experimental solid-state structure of compounds **2a** and **5** (Figure 1) confirmed that carbazoles and benzocarbazoles are skewed with respect to the boron-carbon mesityl moieties (ϕ_1 = 30.5 and ϕ_2 = 36.0° in **2a**, and ϕ_1 = 20.5 and ϕ_2 = 42.2° in **5**), confirming the existence of a rigid and geared structure. In the benzocarbazole compound **5**, the hetero-aromatic ring is also bent away ($\psi_2 = -5.5$) from the steric hindrance caused by the mesityl ring. Very similar torsion angles were observed in compounds **6** and **7**.

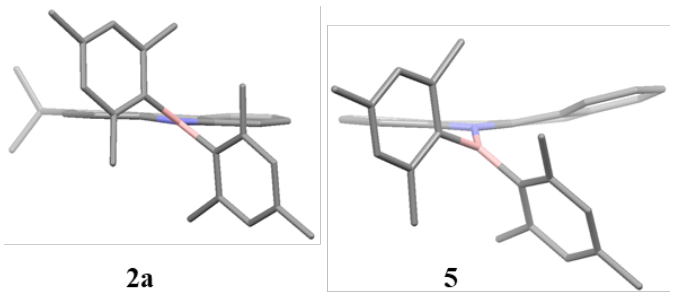

Figure 1. Solid-state structure of compounds **2a** and **5**.

In compound **2a** the B-N bond is slightly shorter (1.45 Å) with respect to the benzocarbazole analogue **5** (1.47 Å). This is most probably a direct consequence of the weaker conjugation due to the distortion of the B-N system, again evident in the calculations of compound **7** (1.46 Å) and **8** (1.47 Å). The -OMe EDG group slightly increases the conjugation by shortening the B-N bond respect to the -CF_3 EWG group.

Stereodynamic analysis

The available stereochemical pathways for enantiomerization and B-N rotation were simulated by DFT calculations. The experimental GS structure suggests that the motions of all the three rings are geared into a single system where the three rings move simultaneously. The stereodynamic behaviour of three- and two-blades propellers has been studied in detail, but the present case is more complicated because two substituents are linked to boron with a σ-bond, whereas the boron-nitrogen bond develops a π-system. The possible TSs for these unusual propeller-like molecules are presented in Scheme 3. Following the "ring flip" nomenclature proposed by Mislow, the TS geometries are identified with respect to the plane containing boron, nitrogen and the two quaternary carbons of mesityl rings (boron is planar). The prefix number indicates the number of rings perpendicular to this plane, whereas the suffix indicates which rings are perpendicular to the reference plane. Therefore, the zero-ring flip TS (**0-RF**) has all the three rings sharing the same plane, whereas the three-ring flip (**3-RF**) has the three rings perpendicular to the reference plane. It has to be underlined that in the case of compounds **2-8** the one-ring flip TS (**1-RF**) has three available geometries (**1-RF-N** with perpendicular carbazole, **1-RF-C** and **1-RF-C'** with perpendicular mesityl ring), instead the two-ring flip TS (**2-RF**) has only two available geometries, thus the total of available TS geometries reaches seven. Due to the huge steric hindrance, the **0-RF** geometry could not be optimized to a TS. All the remaining TS geometries have been identified using DFT at the B3LYP/6-311G(d,p) level of theory. In all the optimized geometries, the single negative frequency corresponding to the TS pathway involved the synchronous movement of all the three rings, thus confirming the geared nature of the whole system. The $\Delta G^{\neq}$ values calculated for **1-RFs** (45.6-62.3 kcal/mol) and for **3-RF** (50.1 kcal/mol) are too high to be accessible. On the contrary, the 2-RFs TS are quite lower in energy, and the two available geometries of 2-RF have different stereochemical effect on the BN branch of the molecule. The **2-RF-CC** TS has global C_s symmetry (C_{2v} in the case of compound **1**). The two mesityl rings reach the geometry by a conrotatory motion that at the same time drives the carbazole ring to be coplanar with the C_b-B-C_a plane. In this geometry the B=N moiety develops the highest available conjugated stabilization because of the parallel disposition of the p_z orbitals on boron and nitrogen. On the other hand, this geometry is sterically disfavoured by the steric clash between the *ortho* methyls and between the hydrogen H1 and H8 of carbazole with the two aromatic mesityl rings. Thus, this TS corresponds to the steric barrier of the B-N bond, and it should raise in energy on raising the skew angle of the

heteroaromatic ring in the GS. This stereochemical event can be observed by NMR by monitoring the *ortho* methyls (and *meta*-hydrogens as well) of the mesityl, and by using the isopropyl group (compounds **2**-**4**, **6**) as a chirality probe. These two possibilities can determine whether the internal motions are fully geared or not. In fact, if the two motions were ungeared, the anisochronicity of the *ortho* methyls should display a different energy barrier with respect to the diastereotopicity of the isopropyl methyl groups that are sensitive only to the molecular chirality.

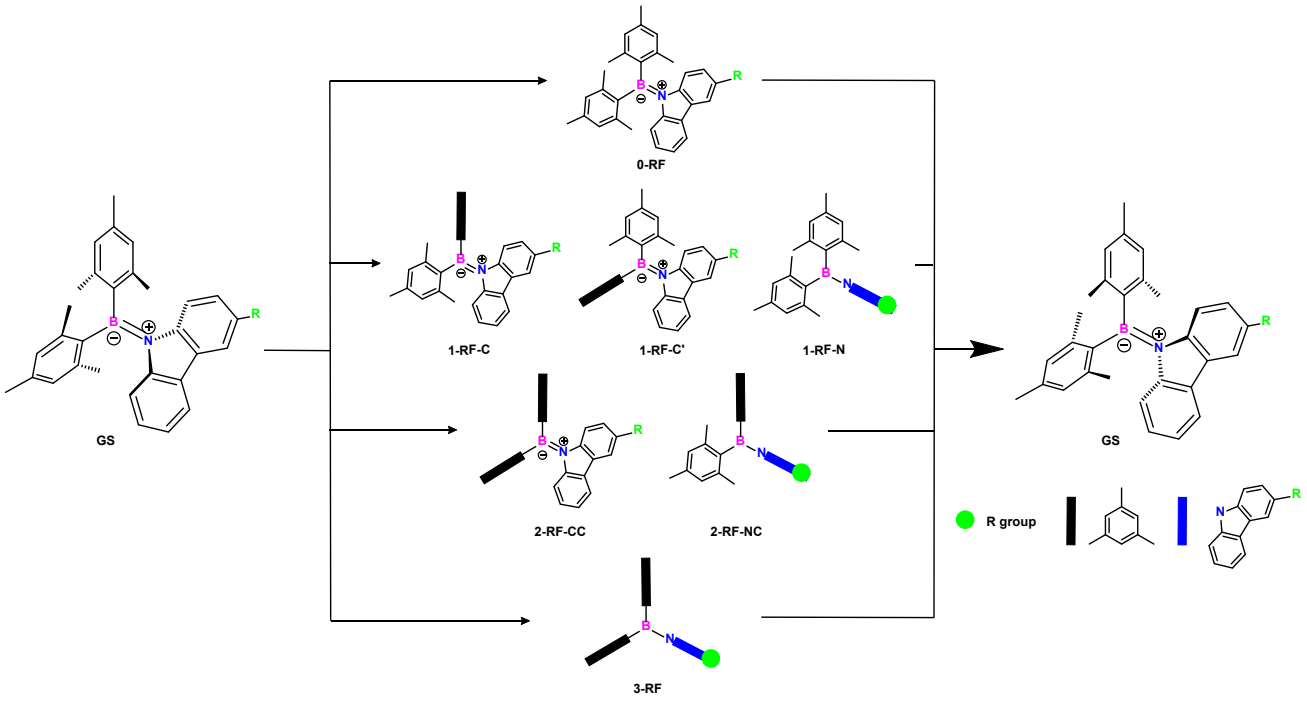

Scheme 3. Available TS geometries for enantiomerization of **2a** (R=*i*-Pr).

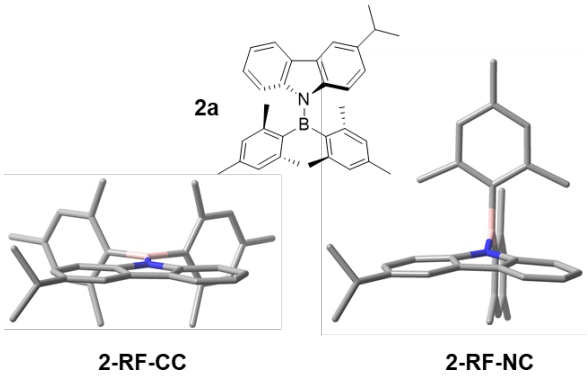

Figure 2. DFT-optimized geometries of the two best TSs of compound **2a** are shown.

The optimized geometry for **2-RF-NC** TS has C_1 symmetry. The two mesityl rings are perpendicular to each other and reach the TS geometry by a disrotatory motion and driving the carbazole plane to be perpendicular to the C_b-B-C_a plane. This geometry implies that the carbazole ring lowers the steric interactions with the mesityl rings, but at the same time the B-N bond completely loses any π contribution (no charge separation) because the two p_z orbitals on boron and nitrogen are perpendicular. This TS corresponds to the conjugative barrier of the B-N bond, with the nitrogen being not exactly planar (357.7°, as the sum of three angles). This pathway can be monitored by the diastereotopicity of the *para*-methyls on the mesityls, that are exchanged by **2-RF-NC** TS, whereas they are not affected in the case of the pathway leading to **2-RF-CC** TS. Among the two geometries, **2-RF-CC** has lower energy (11.1 kcal/mol for **2a**), while **2-RF-NC** has higher energy (22.6 kcal/mol, Table 2).

The higher symmetry of compound **1** allowed to unambiguously determine the activation energy for the steric barrier (**2-RF-CC**). At room temperature the ^{1}H-NMR spectrum of **1** shows a single signal for the four *ortho* methyl that broadens on lowering the temperature, eventually reaching the coalescence at -35 °C (Figure S1). At lower temperatures two anisochronous signals are visible, due to the frozen rotation of the mesityl rings. The presence of two lines for the four methyl groups confirms the C_2 symmetry of the ground state geometry. Line shape simulations at different temperatures allowed to determine a set of rate constants at different temperatures, hence a $\Delta G^{\neq}$ =11.0 ± 0.2 kcal/mol for the dynamic process, in very good agreement with DFT calculations for **2-RF-CC**.

In the case of compound **2a**, the lower symmetry due to the 3-isopropyl moiety implies anysochronicity of all the signals of the mesityls rings, so the ambient temperature ^{1}H-NMR shows two signals for the *ortho*-methyls, and two signals for the *para*-

methyls. On lowering the temperature, the two *ortho*-signals reach the coalescence at -43 °C and eventually split into four signals at -99 °C (Figure 3). Line shape simulation provided a $\Delta G^{\neq}$ =10.9 ± 0.2 kcal/mol for the dynamic process, in analogy with compound **1**. The presence at ambient temperature of two signals for the *para*-methyls indicates that the 180° rotation around the B-N bond is frozen in the NMR timescale, in agreement with the value suggested by DFT calculations (**2-RF-NC** TS energy is 22.6 kcal/mol).

Table 2. Calculated free energy barriers for 2RF-NC and 2-RF-CC TS, and experimental energies determined by NMR (kcal/mol).

Cpd.	2-RF-NC (B-N rotation)		2-RF-CC (B-C rotation)	
	$\Delta G^{\neq}_{calc}$	$\Delta G^{\neq}_{exp}$	$\Delta G^{\neq}_{calc}$	$\Delta G^{\neq}_{exp}$
1	22.4	N.A.	11.1	11.0
2a	24.9	> 22	12.6	10.9
2b	24.6	24.0[a]	12.3	=**2a**
3	25.9	> 22	13.0	10.6
4	24.5	> 22	13.3	11.2
5	20.8	21.5	16.5	15.0
6	21.2	21.7	16.4	16.2
7	21.4	21.6	16.1	15.8
8	21.0	21.0	16.9	15.6

[a] The kinetic analysis was measured starting from ***E*-2b** to ***Z*-2b**.

Although the calculated value is above the limit of the dynamic-NMR technique, an attempt to determine this barrier was done by heating a sample of **2a** to +120 °C in xylene-d_{10}, without any noticeable broadening of the two signals of the *ortho*- and *para*-methyls. Considering the experimental separation of 9.5 Hz at +120 °C for the *para*-methyl signals, and a rate constant lower than 5 s^{-1}, the barrier to B-N rotation is bigger than 22.0 kcal/mol, in full agreement with the DFT calculated value.
However, the conjugative barrier due to 180° rotation of the B-N bond could be measured for compound **2b**, where one mesityl ring was replaced by a 2,6-xilyl ring. This asymmetry on the two rings on boron yields an *E*/*Z* pair of isomers, that could be physically separated by preparative HPLC (Figure S2-S3). By standard kinetic analysis starting from the *E* isomer, a 50:50 thermodynamic ratio was obtained in 1 hour at +51 °C, with experimental energy value of 24.0 kcal/mol (Figure S4). This value is lower than that calculated for the ammonia-borane complex, but still very high, confirming the strength of the π system. When compounds **5-8** are considered, the different steric constrains imposed by the benzo[a]carbazole ring modify the GS geometry, in that the skew angle of the C_eBC_f and C_bNC_a planes raises to 36.5° (as the mean value of ϕ_1 = 28.6° and ϕ_2 = 45.5°, due to nitrogen pyramidality). This larger angle weakens the conjugation between boron and nitrogen, thus implying a lower conjugative barrier and a higher steric barrier. DFT calculations (Table 2) suggested a value of 16.5 kcal/mol for the steric barrier and 18.8 kcal/mol for the conjugative one, both amenable to be observed by Dynamic-NMR.

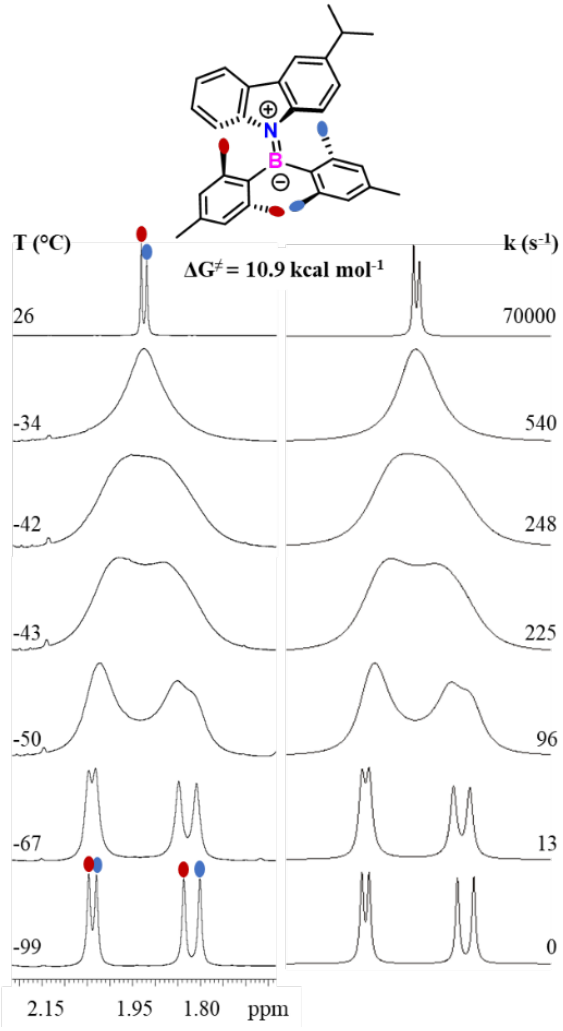

Figure 3. Left: ^{1}H-NMR variable temperature spectra of the *ortho* methyls of compound **2a** (600 MHz in CD_2Cl_2). Right: line shape simulation with the corresponding rate constants.

The ^{1}H-NMR spectrum of compound **6** taken at ambient temperature shows six lines for the methyls of the mesityl rings, and diastereotopic methyls for the isopropyl moiety. Some signals are still broad due to slow exchange, but the ^{1}H spectrum taken at -25 °C shows that all the internal motions are frozen. (Figure 4). The variable temperature NMR spectra were taken in $C_2D_2Cl_4$ in order to increase the temperature and to achieve coalescence of the four methyl signals into two averaged signals, but the huge chemical shift difference between the exchanging signals (410 and 810 Hz) did not allow to observe a single signal within the highest allowed temperature (+120 °C). More conveniently, an exchanging pair of *meta*-hydrogens on one mesityl ring was monitored and a $\Delta G^{\neq}$=16.2 ± 0.2 kcal/mol was derived by line shape simulation (Figure S5 in SI). On the other hand, also the two diastereotopic signals of isopropyl could be monitored for the loss of molecular chirality due to the **2-RF-CC** TS (steric barrier). The chemical shift difference between the two isopropyl methyl is very small (7.0 Hz at -25 °C), and line shape simulation is less accurate in the determination of the activation energy. Nevertheless, the coalescence was observed at +32 °C; hence a $\Delta G^{\neq}$ = 16.2 ± 0.3

kcal/mol was determined, in perfect agreement with the barrier determined on the mesityl signals.

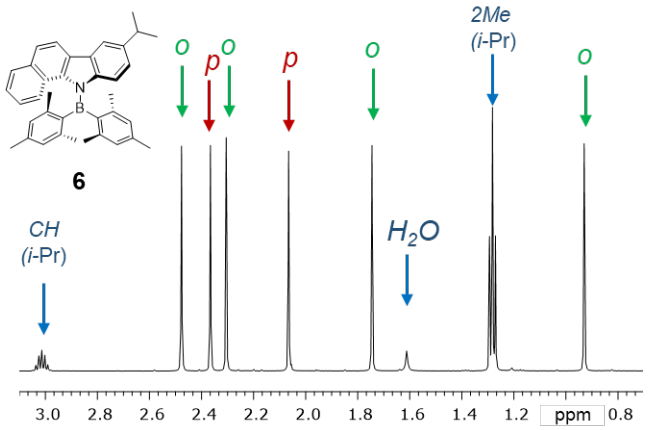

Figure 4. ^{1}H-NMR spectrum of the aliphatic region of **6** at -25 °C (600 MHz in CD_2Cl_2).

The coincidence of the two barriers further confirms the existence of correlated motion. The higher value for steric barrier of **6** with respect to **2** ($\Delta\Delta G^{\neq}$ = 5.2 kcal/mol) is a direct effect of the higher steric hindrance in the planar TS geometry, which forces the benzo[a]carbazole to have a larger skew angle in the GS geometry with respect to the C_eBC_f plane.

At +120°C the ^{1}H-NMR spectrum shows very broad lines for the *ortho* methyls, but the two signals of the *para*-hydrogens of mesityl rings are still sharp. This means that the exchange due to the 180° rotation of the benzo[a]carbazole is still very slow in the NMR timescale, and the barrier cannot be monitored by the dynamic-NMR technique. On the other hand, selective saturation at +120 °C of one of the *p*-methyl signals yielded saturation transfer on the second one, so the rate constant was not negligible. For this reason, 1D-EXSY spectra were acquired at three different temperatures (+93, +98 and +103 °C) to derive three rate constants useful for the determination of the energy barrier, that was found as $\Delta G^{\neq}$ =21.7 ± 0.2 kcal/mol (Figure S6). Despite the small temperature range explored, it should be noted that the activation energy steadily increased from 21.63 kcal/mol at +93 °C to 21.73 kcal/mol at +103 °C thus implying a negative activation entropy ($\Delta S^{\neq}$ = -10 cal/mol·K and $\Delta H^{\neq}$ = 18.0 kcal/mol). This can be attributed to the existence of a strongly organized TS,[18] as suggested by DFT calculation for the **2RF-NC** TS. The value of the conjugative barrier measured for benzocarbazoles **5-8** is ≈3.5 kcal/mol lower with respect to that measured for compound **2a** (Table 2; see Figures S7-S14 of the ESI for the determination of the free energy barrier of each compound). This is because of the larger skew angle of the GS that lowers the π-bond contribution on the BN moiety.

Photophysical Characterization

As often observed for molecules containing a donor (i.e. the substituted carbazole or benzocarbazole) and an acceptor moiety (B-$(Mes)_2$) linked by a single bond, the photoexcitation of the carbazole- and benzocarbazole-boranes described herein may produce an electron transfer process known as TICT (twisted intramolecular charge transfer),[19] which consists of an intramolecular twisting of donor (D) and acceptor (A) units about the N-B single bond. In these D-A systems, the TICT excited states can be tuned by the manipulation of the steric hindrance of the molecule, as well as by the variation of the solvent polarity.[20] On these bases, the influence exerted by the different substituents in compounds **2-8** was investigated through absorption, steady state and time resolved emission spectroscopy. The photophysical behavior of all compounds was analyzed by considering increasingly polar solvents such as hexane, toluene, THF, DCM and acetonitrile. All the relevant data are summarized in Table 3 (absorption, emission and excitation spectra are reported in ESI, Figures S15-S70).

For all the reported compounds, the absorption profiles obtained from the corresponding solutions in various solvents (*i.e.* hexane, toluene, THF, dichloromethane and acetonitrile), invariably exhibited intense π - π* transitions peaking above 300 nm, followed by weaker charge transfer (CT) processes. Even though no appreciable solvatochromism was observed, the position of these CT bands gradually shifts to higher wavelengths according to the series **2a**, **3**, **4** (λ_{abs} *ca.* 320, 330, >350 nm, respectively, see Figure S15, S23 and S31, Table S1), while the replacement of the carbazole moiety with the larger π-system of benzocarbazole (compounds **5-8)** led to the further red-shift of the CT bands up to λ_{abs} = 360 nm (Figure S39, S47, S55 and S63, Table S1).

Upon excitation (λ_{exc} = 350 nm) of the corresponding dilute (10^{-5} M) solutions, all the carbazole and benzocarbazole boranes **2-8** displayed luminescence, with broad and structureless profiles centered between λ_{em} = 430 nm and λ_{em} = 542 nm (Table S1, Figure S15-S70). In all cases, the time resolved analyses of the radiative processes suggested lifetime values (τ) congruent with the fluorescent nature of the emissions. Common to all compounds, a red shift of the emission maxima was observed on going from a not polar solvent such as hexane to acetonitrile (ACN), suggesting how fluorescence likely originates from polar excited states of charge transfer (CT) nature. Consistently with the literature data,[11] compound **1**, which is considered as the reference compound for the whole carbazole series **2a** – **4,** displayed an absorption maximum centered at λ_{abs} = 320 nm both in hexane and THF solution, while emission was found to peak at λ_{em} = 439 in hexane and λ_{em} = 455 nm in THF, respectively. In comparison with **1**, the isopropyl substituted derivative **2a** (R1 = *i*Pr, R2 = H), displayed red shifted emission profile both in hexane (λ_{em} = 446 nm, Stokes shift = 8635 cm^{-1}) and in THF (λ_{em} = 476 nm, Stokes shift = 9860 cm^{-1}). Further red shift was observed with more polar solvents, with the largest bathochromism observed from the acetonitrile solution of **2a** (λ_{em} = 492 nm, Stokes shift = 10635 cm^{-1}) (Table 3). When compared to **2a**, the methoxy substituted compound **3** (R_2 = -OMe) exhibited an additional red shift of the emission maximum, enlightening an effect that became more evident upon increasing the polarity of the solvent ($\Delta\lambda_{em}$ hexane: 30 nm, toluene: 40 nm, DCM: 42 nm, THF: 44 nm, acetonitrile: 50 nm, see Table 3). It is worth noting that among the newly synthesized molecules, compound **3** in acetonitrile solution displayed the largest Stokes shift value of 12700 cm^{-1}. On the other hand, the introduction of the electron-withdrawing

trifluoromethyl substituent in the carbazole skeleton (R_2 = -CF_3, compound **4**) led to emission profiles that were found blue shifted of ca. 20 – 40 nm in comparison to those recorded for compound **3** in the various solvents considered. The presence of the electron withdrawing trifluoromethyl group in compound **4** had a minor impact on its Stokes shift values, which were determined as the less pronounced (i.e. values spanning from 6200 cm^{-1} in hexane and ca. 8400 cm^{-1} in acetonitrile) along the series of the carbazole based derivatives (Table 3). Relative to fluorescence quantum yields, (Φ), the highest value was recorded for compound **4** (29 - 47% *vs* quinine sulphate in 0.05 M H_2SO_4), while lower Φ was determined for **2a** and **3** (see Table 3). A notable exception to this trend was represented by the carbazole derivative **3**, whose quantum yield in THF solution was measured as Φ = 50%. This result might be explained in consideration of the likely extra-stabilization of the B-N bond induced by the presence of THF as the solvent. Taken together, these data suggest that compounds **2a** and **3** likely undergo to a noticeable degree of rearrangement upon excitation, resulting in larger Stokes shifts and reduced Φ values, an effect that might be compatible with the lower overlap of π orbitals.[11,21] In the case of compound **4**, the introduction of an EWG group might account for the reduced Stokes shifts and the concomitant increase of quantum yield (Φ), likely disfavoring the TICT behavior (less-twisted molecules).

Similar trends were observed for the benzocarbazole compounds series **5-8** (Table 3). Compound **5**, which can be considered as the benzofused analogue of **1**, displayed emission maxima peaking between λ_{em} 466 – 504 nm depending on the various solvents employed, with Stokes shifts spanning from ca. 7000 cm^{-1}, as for the solution of **5** in hexane, to ca. 8950 cm^{-1} for the corresponding dichloromethane solution. If compared to compound **1**, the emissions stemming from hexane and THF solutions of **5** were found red shifted by $\Delta\lambda_{em}$ = 27 and 41 nm respectively, an effect that can be ascribed to the presence of the π-extended aromatic system of benzocarbazole. In good agreement with what observed for the carbazole analogues **2a** and **3**, the decoration of the benzocarbazole system with electron donor groups (EDG) such as *i*-Pr (i.e. compound **6**) or -OMe (i.e. compound **7**) involved the red shift of their emission profile with respect to those recorded for compound **5**. In the same comparison, this variation, which appeared more pronounced for compound **7** ($\Delta\lambda_{em}$ = 20-50 nm with respect to **5**, see Table 3 and S48), became more significant upon increasing the solvent polarity. However, for both compounds **6** and **7**, the trend of the Stokes shifts was in line with the values displayed by compound **5**.

As previously discussed for compound **4**, the introduction of a CF_3 group (EWG) in the benzocarbazole backbone (i.e. compound **8**) led to the blue shift ($\Delta\lambda_{em}$ approximately -10 to -30 nm) of the emission maximum with respect to those observed for the unsubstituted benzocarbazole **5** (Δλ hexane: -14 nm, toluene: -16 nm, THF: -10 nm, DCM: -32 nm, acetonitrile: -2 nm), thereby leading to the smallest Stokes shifts (spanning from 6290 cm^{-1} in hexane to 8500 cm^{-1} in acetonitrile) within the benzocarbazole series. This feature might suggest a poorer TICT contribution to the composition of the excited state (see theoretical calculations). Concerning quantum yields (Φ), the lowest values were recorded for **5** (with the exception of Φ_{DCM}= 40%) while the highest are those from **6** (R1 = *i*-Pr). In contrast with the fluorescence efficiency values (Φ ranging from 13 to 34%, Table 3), compound **7** shows Stokes shifts similar to those of **5** and **6**, suggesting that, despite its good emission efficiency, an effective TICT is still taking place.

Although amino-boranes are known to produce TICT excited states due to the increased electronic asymmetry of the B-N moiety in the excited state,[8] the GS geometries of **2-8** are strongly influenced by the different steric hindrance and electronic properties of the carbazole and benzocarbazole rings. As shown above, all compounds showed strong solvatochromic effects, with a red shift when EDG groups are present in the heteroaromatic ring, and a blue shift when EWG groups are present (the isopropyl compounds **2** and **6** are taken as references). In addition, benzocarbazole compounds **5-8** showed smaller Stokes shifts with respect to the corresponding carbazole compounds **1-4**, and a lower energy absorption band. DFT and TD-DFT calculations were used to rationalize the experimental outcomes. All the calculations of the fluorescence cycle were run with the CAM-B3LYP functional, that is known to yield good results in the simulation of the UV absorption spectra.[22] Solvent effects were considered using the IEF-PCM model[23] (full details about the calculation of the whole fluorescence cycle can be found in ESI).

The absorption wavelengths were calculated with TD-DFT for the first three singlet transitions, and the lowest energy one was then considered for the calculation of the fluorescence cycle. In the case of compound **2a**, the lowest UV transition energy was calculated at about 290 nm (4.28 eV) in three different solvents (ΔE_{abs} in Table 4), with small differences between the solvents used in the calculations (oscillator strength ≈ 0.25). TD-DFT calculations confirmed that this transition is mainly due to the HOMO-LUMO transition (81% probability), the HOMO is mainly localized on the carbazole ring, whereas the LUMO is mainly on the $B(Mes)_2$ system, with small contributions of the carbazole (see Table 3 and Figure S71). This transition can be thus assigned to an intramolecular charge-transfer absorption (ICT). In the benzocarbazole **6** (taken as an example for compounds **5-8**), the UV transition is due to two components starting from the HOMO (75%) and HOMO-1 (14%), ending into the LUMO. Both the starting MOs are localized on the benzocarbazole ring, while the LUMO is localized on boron and on the mesityl rings. Hence, also in these cases this transition has ICT features. The geometry optimization of the S^1 geometry of compounds **2-8** showed a large change on ϕ_1 (C-B-N-C torsion angle, $\Delta\phi_1$ in Table 4). Differently from the GS geometry on S^0, both boron and nitrogen are planar on S^1 (sum of angles = 360.0° for nitrogen and 359.8° for boron). Due to the loss of π contribution, the B-N bond length is elongated to 1.54 Å (1.46 Å in the GS on S^0), as usual in TICT excited states. The MO involved in the fluorescence emission are the same of the absorption, but the LUMO shape is now completely shifted onto the $B(Mes)_2$ moiety.

ARTICLE

Table 3: Photophysical data summary for compounds **2** –**8**

Compound	Solvent	Absorption	Emission (298 K)						Emission Neat Solid Matrix (298 K)	
		λ(nm) 10^{-4}ε ($cm^{-1}M^{-1}$)	λ_{em} (nm)	τ_{ox} (ns)	Φ_{ox}[a] (%)	K_r[b] (s^{-1})	K_{nr}[b] (s^{-1})	Stokes shift (cm^{-1})	λ_{em} (nm)	τ (ns)
2a	Hex	322 (1.58)	446	5	8	$1.6*10^7$	$1.8*10^8$	8635	430	5
	Toluene	323 (1.51)	460	9	23	$2.7*10^7$	$8.9*10^7$	9220		
	THF	324 (1.71)	476	12	35	$2.8*10^7$	$5.2*10^7$	9860		
	DCM	324 (1.79)	482	15	29	$1.9*10^7$	$4.7*10^7$	10120		
	CH_3CN	323 (1.49)	492	13	20	$1.5*10^7$	$6.0*10^7$	10630		
3	Hex	320 (1.45), 334 (1.73)	476	9	22	$2.4*10^7$	$8.6*10^7$	8930	436	6
	Toluene	322 (1.56), 335 (1.81)	500	13	29	$2.2*10^7$	$5.5*10^7$	9850		
	THF	336 (1.84)	520	19	50	$2.6*10^7$	$2.6*10^7$	10530		
	DCM	323 (1.71), 336 (1.92)	524	17	27	$1.6*10^7$	$4.3*10^7$	10680		
	CH_3CN	321 (1.55), 334 (1.72)	542	10	12	$1.2*10^7$	$8.8*10^7$	12700		
4	Hex	335 (0.68), 352 (0.57)	450	6	29	$4.8*10^7$	$1.2*10^8$	6190	438	9
	Toluene	337 (0.65), 353 (0.60)	470	12	47	$4.1*10^7$	$4.6*10^7$	7050		
	THF	337 (0.71), 353 (0.62)	484	15	33	$2.2*10^7$	$4.5*10^7$	7670		
	DCM	336 (0.75), 353 (0.66)	486	17	36	$2.1*10^7$	$3.8*10^7$	7750		
	CH_3CN	335 (0.61), 352 (0.55)	500	15	36	$2.4*10^7$	$4.4*10^7$	8410		
5	Hex	334 (0.82), 354 (0.65)	466	10	9	$9.3*10^6$	$9.4*10^7$	7000	448	6
	Toluene	336 (0.77), 353 (0.62)	486	13	14	$1.1*10^7$	$6.9*10^7$	7750		
	THF	336 (0.77), 353 (0.62)	496	14	14	$9.8*10^6$	$6.0*10^7$	8170		
	DCM	338 (0.71), 353 (0.68)	516	19	40	$2.1*10^7$	$3.2*10^7$	8950		
	CH_3CN	335 (0.75), 350 (0.62)	504	15	10	$6.6*10^6$	$6.0*10^7$	8730		
6	Hex	340 (0.95), 355 (0.89)	466	10	20	$2.0*10^7$	$8.0*10^7$	6700	450	5.6
	Toluene	342 (0.94), 355 (0.91)	488	13	30	$2.2*10^7$	$5.2*10^7$	7680		
	THF	341 (0.82), 354 (0.80)	504	20	49	$2.5*10^7$	$2.6*10^7$	8410		
	DCM	341 (0.82), 354 (0.80)	510	19	25	$1.3*10^7$	$3.9*10^7$	8640		
	CH_3CN	341 (0.71), 354 (0.68)	520	14	21	$1.5*10^7$	$5.6*10^7$	9020		
7	Hex	320 (2.17), 344 (1.22), 361 (1.06)	478	9	15	$1.7*10^7$	$9.4*10^7$	6780	466	11
	Toluene	320 (2.14), 345 (1.12), 360 (1.00)	498	12	23	$1.9*10^7$	$6.4*10^7$	7700		
	THF	320 (2.07), 345 (1.17), 362 (1.05)	516	19	34	$1.8*10^7$	$3.5*10^7$	8250		
	DCM	322 (1.58), 344 (0.89), 363 (0.80)	520	17	18	$1.1*10^7$	$4.8*10^7$	8320		
	CH_3CN	320 (2.21), 346 (1.13), 361 (1.00)	530	13	13	$1.0*10^7$	$6.7*10^7$	8830		
8	Hex	335 (0.99), 352 (1.01)	452	6	11	$1.7*10^7$	$1.4*10^8$	6280	428	2
	Toluene	337 (1.07), 354 (1.06)	470	11	20	$1.8*10^7$	$7.1*10^7$	6970		
	THF	337 (1.23), 353 (1.02)	486	15	25	$1.7*10^7$	$5.1*10^7$	7750		
	DCM	337 (1.23), 353 (1.16)	484	17	25	$1.4*10^7$	$4.3*10^7$	7670		
	CH_3CN	337 (1.21), 352 (1.16)	502	15	16	$1.1*10^7$	$5.6*10^7$	8490		

[a]: vs Quinine Sulphate/0.05 M H_2SO_4, Φ = 0.53[24]; [b]: $K_r = \Phi/\tau(s)$, $K_{nr} = (1-\Phi)/\tau(s)$.

Table 4. Summary of dihedral angle variation between the optimized S° and S^1 optimized geometries of compounds **2-8**, together with calculated and experimental Stoke Shift. Calculations at the PCM-CAM-B3LYP/6-31G(d) level for geometry optimization, and PCM-CAM-B3LYP/6-31+G(d,p) level for vertical transitions.

Compd.	PCM Solvent	$\Delta\phi_1$ calc. (°)	ΔE_{abs} (eV)	ΔE_{emi} (eV)	ΔE_{S1} (eV)	ΔE_{S0} (eV)
2a	Hexane	33.3	4.27	2.88	0.89	0.50
	THF	32.4	4.30	2.64	1.11	0.55
	ACN	31.9	4.32	2.54	1.20	0.58
***E*-2b**	Hexane	32.9	4.28	2.83	0.92	0.52
	THF	31.9	4.29	2.58	1.15	0.57
	ACN	31.8	4.31	2.47	1.24	0.60
***Z*-2b**	Hexane	33.2	4.26	2.83	0.91	0.52
	THF	32.4	4.29	2.57	1.15	0.57
	ACN	31.9	4.31	2.47	1.24	0.60
3	Hexane	34.8	4.16	2.64	0.94	0.58
	THF	33.7	4.19	2.33	1.22	0.65
	ACN	33.4	4.22	2.21	1.32	0.68
4	Hexane	29.1	4.25	3.04	0.74	0.47
	THF	28.1	4.26	2.79	0.96	0.51
	ACN	28.1	4.29	2.69	1.07	0.54
5	Hexane	27.0	3.89	2.80	0.68	0.40
	THF	25.6	3.91	2.52	0.92	0.46
	ACN	24.2	3.92	2.40	1.02	0.50
6	Hexane	27.3	3.89	2.79	0.69	0.40
	THF	25.4	3.90	2.53	0.91	0.46
	ACN	24.9	3.91	2.41	1.01	0.49
7	Hexane	27.6	3.87	2.76	0.71	0.41
	THF	26.4	3.89	2.46	0.95	0.47
	ACN	25.8	3.90	2.34	1.05	0.51
8	Hexane	24.9	3.91	2.90	0.62	0.40
	THF	23.3	3.94	2.59	0.88	0.46
	ACN	22.5	3.95	2.46	0.99	0.50

The smaller Stokes shifts of compounds **5-8** compared to **2-4** is rationalized by considering the geometry difference between the GS on S° and in the S^1 optimized geometry ($\Delta\phi_1$ in Table 4). While the S^1 optimized geometry is very similar for all compounds ($\phi_1 \approx 60°$), the starting geometries are quite different because of the different steric hindrance exerted by the carbazole (compounds **2-4**) and benzocarbazole (**5-8**). Both the absorption wavelength and Stokes shift are therefore influenced by two opposite contributions. On one side the absorption band is red shifted by the larger π system of benzocarbazole, while the Stokes shift is reduced because of the smaller energy gain during geometry rearrangement in the excited state. The effect of substituents on the heteroaromatic ring (-OMe and $-CF_3$) can be rationalized by considering how they modify the shape of S^1 (Table 4). Compounds **3** and **7** (-OMe) have, within their class and solvent, the lowest value of ΔE_{emi}, while compounds **4** and **8** ($-CF_3$) show the highest value. The term ΔE_{abs} turns out to be much less sensitive to substituents than ΔE_{emi}. The OMe substituent increases conjugation and favours the charge transfer from the heteroaromatic ring to the boron atom, thus lowering the HOMO-LUMO gap, with a greater stabilization of the GS on S^1 compared to S° (as observable from the terms ΔE_{S1} in Table 4). On the contrary, the electron-withdrawing CF_3 substituent (**4** and **8**) disfavours the TICT character of the ES and leads to a smaller ΔE_{S1}, thus increasing the emission energy ΔE_{emi}. The substituent impact on the fluorescent features is therefore larger on the carbazole series because of the larger TICT rearrangement in the excited state.

Dynamic properties of the excited state

The two isomers of compound **2b** offered a noticeable occasion to monitor the dynamic features of the excited states, thus to evaluate the conjugative contributions. In fact, the charge separation and TICT process weaken the B-N π-bond and drive the GS geometry on S^1 towards the transition state geometry for E/Z isomerization (**2RF-NC** in Scheme 2). The resulting isomerization barrier should be therefore largely reduced. The samples used for fluorescence measurements of **2b** were checked by NMR before and after 10 min UV irradiation, without noticeable isomerization. This implies that the rotational barrier on S^1 is still high enough to avoid isomerism in the ns timescale. An estimate of the rotational barrier was obtained by geometry optimization of the transition state on S^1 by using TD-DFT at the same level used for the fluorescence cycle (CAM-B3LYP/6-31G(d), THF as the solvent), yielding a value of 9.4 kcal/mol, corresponding to a lifetime of ≈900 ns at +25°C. The geometry of the TS on S^1 in very similar to that on S^0, but with a slightly longer B-N bond (1.54 Å vs 1.52 Å).

Conclusions

We have investigated the stereodynamic properties of two series of aminoboranes bearing carbazole and benzocarbazole as the donor heterocycle. It has been shown that the dynamic properties of the B-N bond and the GS geometries lead to the formation of conformational enantiomers, with an enantiomerization barriers due to a correlated motion of the two aryl rings on boron and the heterocycle. The B-N π-contribution has been measured as 24 kcal/mol in the carbazole series (**2-4**) and 21.7 kcal/mol in the benzocarbazole series (**5-8**). This stereodynamic rearrangement happens with a gear-like process too. The difference in the GS geometries of the two series led to strong differences in the fluorescence spectra, due to different geometric rearrangements in the excited state. Stokes shifts, as large as 12700 cm^{-1} nm, were observed in the carbazole series, with quantum yields up to 50%. By monitoring compound 2b, it has been found that the π-contribution to the B-N bond in the excited state is not completely cancelled by the TICT process, being E/Z isomers conformationally stable under UV irradiation.

Experimental

General. Full experimental procedures for the synthesis and spectroscopic characterization of compounds **2-8** and intermediates can be found in the ESI.

General procedure for amino-borane synthesis

In a 25 mL oven-dried reaction vessel, 2-bromomesitylene (0.90 mL, 6 mmol), magnesium (0.2 g), dry THF (6 mL) and a tip of iodine were added under nitrogen flow, stirred and left to reflux for 2 hours. The Grignard solution was then cooled to -78 °C and BF_3OEt (0.41 mL, 3 mmol) was added dropwise and then stirred for 12 hours and gradually warming up until room temperature. In a second oven-dried reaction vessel containing carbazole (or benzocarbazole, 3 mmol) and dry THF (6 mL), KHMDS (0.5 M solution, 3 mmol) was added dropwise and the solution was stirred at ambient temperature for 1h. The first solution of Mes_2BF was then added dropwise and the mixture was then refluxed for 4h. After cooling to room temperature, the reaction was quenched with DCM, filtered on Celite® and purified by chromatography separation (silica gel, Hexane/DCM= 7:3), followed by crystallization in DCM/acetonitrile.

Dynamic-NMR

The low-temperature NMR spectra were obtained by using a flow of dry nitrogen which entered into an inox steel heat exchanger immersed in liquid nitrogen and connected to the NMR probe head by a vacuum-insulated transfer line. The 600 MHz ^1H spectra were acquired using a 5 mm direct probe.

High-temperature NMR spectra were obtained with the same probe by preheating the nitrogen flow to 60 °C with an FTS thermostatic unit. Temperature calibrations were performed before the experiments, using a digital thermometer and a Cu/Ni thermocouple placed in an NMR tube filled with isopentane or 1,1,2,2-tetrachloroethane (for the low and high temperature range, respectively). The uncertainty in the temperature measurements can be estimated from the calibration curve as ±1 °C. Line shape simulations were performed using a PC version of the QCPE DNMR6 program.[25] Electronic superimposition of the original and the simulated spectra enabled the determination of the most reliable rate constants at a few different temperatures. These constants provided the free energies of activation ($\Delta G^{\neq}$) by means of the Eyring equation.

Photophysical Measurements

Absorption spectra were recorded at room temperature using a Cary 100 UV/vis spectrometer, Agilent. Uncorrected steady-state emission and excitation spectra were recorded on an Edinburgh FLSP920 spectrometer equipped with a 450 W xenon arc lamp, double excitation and single emission monochromators, and a Peltier-cooled Hamamatsu R928P photomultiplier tube (185−850 nm). Emission and excitation spectra were acquired with a cut-off filter (340 nm) and corrected for source intensity (lamp and grating) and emission spectral response (detector and grating) by a calibration curve supplied with the instrument. The wavelengths for the emission and excitation spectra were determined using the absorption maxima of the MLCT transition bands (emission spectra) and at the maxima of the emission bands (excitation spectra). Quantum yields (Φ) were determined using the optically dilute method by Crosby and Demas[26] at excitation wavelength obtained from absorption spectra on a wavelength scale [nm] and compared to the reference emitter by the following equation:[27]

$$\phi_s = \phi_r \left[\frac{A_r(\lambda_r)}{A_s(\lambda_s)}\right]\left[\frac{I_r(\lambda_r)}{I_s(\lambda_s)}\right]\left[\frac{n_s^2}{n_r^2}\right]\left[\frac{D_s}{D_r}\right]$$

where A is the absorbance at the excitation wavelength (λ), I is the intensity of the excitation light at the excitation wavelength (λ), n is the refractive index of the solvent, D is the integrated intensity of the luminescence, and Φ is the quantum yield. The subscripts r and s refer to the reference and the sample, respectively. A stock solution with an absorbance > 0.1 was prepared, then a 10 times diluted solution was obtained. The Lambert-Beer law was assumed to remain linear at the concentration of the solutions. The degassed measurements were obtained after the solutions were bubbled for 10 minutes under Ar atmosphere, using a septa-sealed quartz cell. Air-equilibrated Quinine Sulphate in 0.05 M H_2SO_4 ($\Phi = 0.52$)[24] was used as reference. The quantum yield determinations were performed at identical excitation wavelengths for the sample and the reference, therefore deleting the I(λr)/I(λs) term in the equation. Emission lifetimes (τ) were determined with the single photon counting technique (TCSPC) with the same Edinburgh FLSP920 spectrometer using pulsed picosecond LED (EPLED 340, FWHM < 800 ps) as the excitation source, with repetition rates between 1 kHz and 1 MHz, and the above-mentioned R928P PMT as detector. The goodness of fit was assessed by minimizing the reduced $\chi 2$ function and by visual inspection of the weighted residuals. To record the neat solid matrix luminescence spectra, the samples were placed on carbon tape adhered on a quartz cuvette for solid samples. The solvent used in the preparation of the solutions for the photophysical investigations was of spectrometric grade. Experimental uncertainties are estimated to be ±8% for lifetime determinations, ±20% for quantum yields, and ±2 nm and ±5 nm for absorption and emission peaks, respectively.

Calculations

All the calculations were run using the Gaussian 16 suite of programs.[17] Ground states and transition states geometry optimizations employed the B3LYP hybrid HF-DFT functional[28] and the 6-31G(d) basis set. The analysis of the vibrational frequencies for the optimized structures showed the absence of imaginary frequencies for the ground states, and the presence of one imaginary frequency for each transition state. Visual inspection of the corresponding normal mode[29] validated the identification of the transition states. If not differently stated, the reported energy values derive from ZPE-corrected energies, with unscaled frequencies. The fluorescence cycle was calculated using the CAM-B3LYP functional. Geometry

optimization on S° and S^1 were run using the 6-31G(d) basis set, whereas the larger 6-31+G(d,p) basis set was used for the calculation of the vertical transition energies. For compound **2** it was checked that the use of the smaller basis set in the geometry optimization yielded GS geometries superimposable with those optimized with the larger basis set (both on S^0 and S^1), but with much shorter computational time.

Author Contributions

M.M. and A.M. designed the project; M.M., D.P. and S.F. prepared the compounds and performed NMR analysis; D.P., S.G. and V.F. performed fluorescence measurements and theoretical calculations. A.M., S.S. and M.M. wrote the manuscript.

Conflicts of interest

There are no conflicts to declare.

Acknowledgements

The University of Bologna is gratefully acknowledged (RFO Funds 2018 and 2019). AM, MM and DP thank Alchemy SrL, Bologna, for a generous gift of chemicals.

Notes and references

§ CIF files of compounds **2** and **5-7** have been deposited within the CCDC database with deposition numbers 2080357-2080360.

1 H-J. Li, S. K. Mellerup, X. Wang, and S. Wang, D–π–A Triarylboranes as Reversible Fluorescent Probes for CO2 and Temperature, *Org. Lett.* 2019, **21**, 2838.

2 a) S. Wang, Luminescence and electroluminescence of Al(III), B(III), Be(II) and Zn(II) complexes with nitrogen donors, *Coord. Chem. Rev.*, 2001, **215**, 79; b) Q. D. Liu, M. S. Mudadu, R. Thummel, Y. Tao and S.Wang, From Blue to Red: Syntheses, Structures, Electronic and Electroluminescent Properties of Tunable Luminescent N,N Chelate Boron Complexes, *Adv. Funct. Mater*., 2005, **15**, 143; c) Y. Cui, Q. D. Liu, D. R. Bai, W. L. Jia, T. Ye and S. Wang, Organoboron Compounds with an 8-Hydroxyquinolato Chelate and Its Derivatives: Substituent Effects on Structures and Luminescence, *Inorg. Chem.*, 2005, **44**, 601; d) Y. Qin, I. Kiburu, S. Shah and F. Jäkle, Luminescence Tuning of Organoboron Quinolates through Substituent Variation at the 5-Position of the Quinolato Moiety, *Org. Lett.*, 2006, **8**, 5227; e) Q.G. Wu, M. Esteghamatian, N. X. Hu, Z. Popovic, G. Enright, Y. Tao, M. D'Iorio and S. Wang, Synthesis, Structure, and Electroluminescence of BR2q (R = Et, Ph, 2-Naphthyl and q = 8-Hydroxyquinolato), *Chem. Mater.*, 2000, **12**, 79; f) H. Y. Chen, Y. Chi, C. S. Liu, J. K. Yu, Y. M. Cheng, K. S. Chen, P. T. Chou, S. M. Peng, G. H. Lee, A. J. Carty, S. J. Yeh and C. T. Chen, Rational Color Tuning and Luminescent Properties of Functionalized Boron-Containing 2-Pyridyl Pyrrolide Complexes, *Adv. Funct. Mater.*, 2005, **15**, 567.

3 a) K.K. Neena, P. Sudhakar, K. Dipak and P. Thilagar, Diarylboryl-phenothiazine based multifunctional molecular siblings, *Chem. Commun.*, 2017, **53**, 3641; b) C. Arivazhagan, A. Maity, K. Bakthavachalam, A. Jana, S.K. Panigrahi, E. Suresh, A. Das and S. Ghosh, Phenothiazinyl Boranes: A New Class of AIE Luminogens with Mega Stokes Shift, Mechanochromism, and Mechanoluminescence, *Chem. Eur. J.*, 2017, **23**, 7046.

4 M. M. Alam, M. Chattopadhyaya and S. Chakrabarti, A critical theoretical study on the two-photon absorption properties of some selective triaryl borane-1-naphthylphenyl amine based charge transfer molecules, *Phys. Chem. Chem. Phys.,* 2011, **13**, 9285.

5 Y-G. Shi, J-W. Wang, H. Li, G-F Hu, X. Li, S. K. Mellerup, N. Wang, T. Peng and S. Wang., A simple multi-responsive system based on aldehyde functionalized amino-boranes, *Chem. Sci.,* 2018, **9**, 1902.

6 For reviews see a) Z. Zhao, H. Zhang, J. W. Y. Lam and B. Z. Tang, Aggregation-Induced Emission: New Vistas at the Aggregate Level, *Angew. Chem. Int. Ed.* 2020, **29**, 9888; b) Y. Hong, J. W. Y. Lam and B. Z. Tang., Aggregation-induced emission, *Chem. Soc. Rev.* 2011, **40**, 5361.

7 P. Ganesan, D-G. Chen, W-C. Chen, P. Gnanasekaran, J-A. Lin, C-Y. Huang, M-C. Chen, C-S. Lee, P-T. Chou and Y. Chi., Methoxy substituents activated carbazole-based boron dimesityl TADF emitters, *J. Mat. Chem. C,* 2020, **8**, 4780.

8 J. Wang, Y. Wang, T. Taniguchi, S. Yamaguchi and S. Irle, Substituent Effects on Twisted Internal Charge Transfer Excited States of N-Borylated Carbazoles and (Diphenylamino)boranes, *J. Phys. Chem. A* 2012**, 116**, 1151.

9 a) J. F. Blount, P. Finocchiaro, D. Gust and K. Mislow, Conformational analysis of triarylboranes, *J. Am. Chem. Soc.* 1973, **95**, 7019; b) K. Mislow, Stereochemical consequences of correlated rotation in molecular propellers, *Acc. Chem. Res.* 1976, **9**, 26.

10 D. J. Grant and D. A. Dixon, σ- and π-Bond Strengths in Main Group 3−5 Compounds, *J. Phys. Chem. A* 2006, **110**, 12955.

11 T. Taniguchi, J. Wang, S. Irle and S.Yamaguchi, TICT fluorescence of N-borylated 2,5-diarylpyrroles: a gear like dual motion in the excited state, *Dalton Trans.*, 2013, **42**, 620.

12 S. Grilli, L. Lunazzi, A. Mazzanti, D. Casarini and C. Femoni, Conformational studies by dynamic NMR. 78. Stereomutation of the helical enantiomers of trigonal carbon diaryl-substituted compounds: dimesitylketone, dimesitylthioketone, and dimesitylethylene, *J. Org. Chem.,* 2001, **66**, 488.

13 E.L. Eliel and S.H. Wilen, in *Stereochemistry of Organic Compounds*, J.Wiley and Sons, New York, 1994, Chapter 14-6, pp. 1156-1163.

14 a) A. Mazzanti, M. Boffa, E. Marotta and M. Mancinelli, Axial Chirality at the Boron–Carbon Bond: Synthesis, Stereodynamic Analysis, and Atropisomeric Resolution of 6-Aryl-5,6-dihydrodibenzo[c,e][1,2]azaborinines, *J. Org. Chem.,* 2019, **84**, 12253; b) A. Mazzanti, E. Mercanti and M. Mancinelli, Axial Chirality about Boron–Carbon Bond: Atropisomeric Azaborines, *Org. Lett.,* 2016, **18**, 2692.

15 M.P. Johansson, and J. Olsen, Torsional Barriers and Equilibrium Angle of Biphenyl: Reconciling Theory with Experiment, *J. Chem. Theory Comput.,* 2008, **4**, 1460.

16 a) V. Balzani, A. Credi and M. Venturi, in *Molecular Devices and Machines –Concepts and Perspectives for the Nanoworld*, Wiley-VCH, Weinheim, 2008; b) S. Erbas-Cakmak, D. A. Leigh, C. T. McTernan and A. L. Nussbaumer, Artificial Molecular Machines, *Chem. Rev.*, 2015, **115**, 10081; c) S. Kassem, T. van Leeuwen, A. S. Lubbe, M. R. Wilson, B. L. Feringa and D. A. Leigh, Artificial molecular motors, *Chem. Soc. Rev.*, 2017, **46**, 2592; d) J. Groppi, M. Baroncini, M. Venturi, S. Silvi and A. Credi, Design of photo-activated molecular machines: highlights from the past ten years, *Chem. Commun.*, 2019, **55**, 12595.

17 Gaussian 16, Revision A.03, M. J. Frisch, G. W. Trucks, H. B. Schlegel, G. E. Scuseria, M. A. Robb, J. R. Cheeseman, G. Scalmani, V. Barone, G. A. Petersson, H. Nakatsuji, X. Li, M. Caricato, A. V. Marenich, J. Bloino, B. G. Janesko, R. Gomperts, B. Mennucci, H. P. Hratchian, J. V. Ortiz, A. F. Izmaylov, J. L. Sonnenberg, D. Williams-Young, F. Ding, F. Lipparini, F. Egidi,

J. Goings, B. Peng, A. Petrone, T. Henderson, D. Ranasinghe, V. G. Zakrzewski, J. Gao, N. Rega, G. Zheng, W. Liang, M. Hada, M. Ehara, K. Toyota, R. Fukuda, J. Hasegawa, M. Ishida, T. Nakajima, Y. Honda, O. Kitao, H. Nakai, T. Vreven, K. Throssell, J. A. Montgomery, Jr., J. E. Peralta, F. Ogliaro, M. J. Bearpark, J. J. Heyd, E. N. Brothers, K. N. Kudin, V. N. Staroverov, T. A. Keith, R. Kobayashi, J. Normand, K. Raghavachari, A. P. Rendell, J. C. Burant, S. S. Iyengar, J. Tomasi, M. Cossi, J. M. Millam, M. Klene, C. Adamo, R. Cammi, J. W. Ochterski, R. L. Martin, K. Morokuma, O. Farkas, J. B. Foresman and D. J. Fox, Gaussian, Inc., Wallingford CT, 2016.

18 E. Masson, Torsional barriers of substituted biphenyls calculated using density functional theory: a benchmarking study, *Org. Biomol. Chem.*, 2013, **11**, 2859.

19 a) C. Cornelissen-Gude and W. Rettig, An Experimental and ab Initio CI Study for Charge Transfer Excited States and Their Relaxation in Pyrroloborane Derivatives, *J. Phys. Chem. A*, 1999, **103**, 4371; b) Y. Cui, F. Li, Z.-H. Lu and S. Wang, Three-coordinate organoboron with a B=N bond: substituent effects, luminescence/electroluminescence and reactions with fluoride, *Dalton Trans.*, 2007, 2634; c) V. Bonacic-Koutecky and J. Michl, Charge-transfer-biradical excited states: relation to anomalous fluorescence." Negative" S1-T1 splitting in twisted aminoborane, *J. Am. Chem. Soc.*, 1985, **107**, 1765.

20 S. Sasaki, G. P. C. Drummen and G-I. Konishi, Recent advances in twisted intramolecular charge transfer (TICT) fluorescence and related phenomena in materials chemistry, *J. Mater. Chem. C,* 2016, **4**, 2731.

21 M. V. Auweraer, Z. R. Grabowski and W. Rettig, Molecular structure and the temperature-dependent radiative rates in Twisted Intramolecular Charge-Transfer and exciplex systems, *J. Phys. Chem.*, 1991, **95**, 2083.

22 a) T. Yanai, D. Tew and N. Handy, A new hybrid exchange–correlation functional using the Coulomb-attenuating method (CAM-B3LYP), *Chem. Phys. Lett.*, 2004, **393***,* 51; b) D. Jacquemin, A. Planchat, C. Adamo and B. Mennucci, TD-DFT Assessment of Functionals for Optical 0–0 Transitions in Solvated Dyes, *J. Chem. Theory Comput.* 2012, **8**, 2359.

23 a) B. Mennucci, Polarizable continuum model, *WIREs Comput. Mol. Sci.* 2012, **2**, 386; b) J. Tomasi, B. Mennucci and R. Cammi, Quantum Mechanical Continuum Solvation Models, *Chem. Rev.* 2005, **105***,* 2999.

24 A. M. Brouwer, Standards for photoluminescence quantum yield measurements in solution (IUPAC Technical Report), *Pure Appl. Chem*., 2001, **83**, 2213.

25 J.H. Brown and C.H. Bushweller, QCPE Bulletin, 1983, **3**, 103. A copy of the program is available on request from the authors (A.M. and M.M.).

26 G. A. Crosby and J. N. Demas, Measurement of photoluminescence quantum yields. Review, *J. Phys. Chem.,* 1971, **75**, 991.

27 D.F. Eaton, Reference materials for fluorescence measurement, *Pure Appl. Chem*., 1988, **60**, 1107.

28 a) C. Lee, W. Yang, R.G. Parr, Development of the Colle-Salvetti correlation-energy formula into a functional of the electron density, *Phys. Rev. B* 1988, **37**, 785; b) A.D. Becke, Density-functional thermochemistry. III. The role of exact exchange, *J. Chem. Phys.* 1993, **98**, 5648; c) P.J. Stephens, F.J. Devlin, C.F. Chabalowski and M. J. Frisch, Ab Initio Calculation of Vibrational Absorption and Circular Dichroism Spectra Using Density Functional Force Fields, *J. Phys. Chem*. 1994, **98**, 11623.

29 GaussView 6.0.16, Semichem Inc., 2016**.**

